LUMINOSITY LIMITATIONS AT HADRON COLLIDERS

F. Zimmermann, CERN, Geneva, Switzerland

Abstract

I discuss fundamental luminosity limitations at hadron colliders, addressing head-on and long-range beam-beam interaction, empirical scaling, synchrotron radiation, intrabeam scattering, dynamic evolution during the store, flat beams, heat load, power consumption, and electron cloud. Parameters of past or operating colliders — ISR, SPS, Tevatron, RHIC — , are compared with the LHC and further extrapolated to an LHC upgrade and to the VLHC.

1 PAST AND FUTURE

So far 4 hadron colliders have been in operation (ISR, SPS, Tevatron, and RHIC) and a 5th is under construction (LHC). The CERN ISR started operation in 1970. A double ring collider, it reached a peak luminosity of 2.2×10^{32} cm^{-2}s^{-1} and a maximum beam energy of 31 GeV with coasting beams of 38–50 A current each. The ISR luminosity was limited by space-charge tune shift and spread, coherent beam-beam effects, proton-electron two-stream instabilities, pressure bumps, detector background, and accumulation efficiency [1]. The ISR also produced the first $\mathrm{p\bar{p}}$ collisions, and, when operated with bunched beams, it reached a beam-beam tune shift of $\xi = 0.0035$ per interaction point (IP) with 8 crossings [2]. The second hadron collider was the CERN $\mathrm{Sp\bar{p}S}$ operating since 1981 at ten times higher energy than the ISR. The $\mathrm{Sp\bar{p}S}$ discovered the W and Z bosons. Its luminosity was limited by beam-beam interaction, loss of longitudinal Landau damping, number of available antiprotons, hourglass effect, and intrabeam scattering [3]. Typical beam-beam tune shift was $\xi = 0.005$ at each of three interaction points. The FNAL Tevatron is the first collider based on superconducting magnets. Colliding-beam operation here started in 1987 [4]. Tevatron luminosity is limited by antiproton intensity, beam-beam interaction including long-range effects, luminosity lifetime, number of events per crossing, and intrabeam scattering. It reached an antiproton beam-beam tune shift above $\xi = 0.009$. The Tevatron discovered the b and t quarks. RHIC at BNL, the first heavy-ion collider, delivers luminosity since 2000. The main limiting factor is intrabeam scattering. Other factors again are beam-beam interaction, luminosity lifetime, and the number of events per crossing. LHC will start operation in 2006. As for the Tevatron, limits will be beam-beam interaction, luminosity lifetime, and events per crossing. Possibly, in addition, the electron cloud produced by photoemission or beam-induced multipacting [5], and local magnet quenches induced by the collision products [6] may prove important. Centre-of-mass energy is 14 TeV and design luminosity 10^{34} cm^{-2}s^{-1}. The LHC will be the first machine where radiation damping is stronger than intrabeam scattering. The scarcity of antiprotons is no longer a problem, as LHC and all future machines will collide protons on protons. If stronger magnets become available in the future, the LHC energy could be raised, *e.g.*, by a factor of 2. In the following, we call this energy increase, combined with a luminosity upgrade to 10^{35} cm^{-2}s^{-1}, the 'LHC-II'. Finally, there exist low-field (LF) and high-field (HF) design concepts for a Very Large Hadron Collider (VLHC) [7], reaching an energy of 100 TeV centre of mass, and the Eloisatron Project [8].

Tables 1 and 2 list parameters for all these colliders, except for the ISR and the Eloisatron. The ISR was a rather special machine. The properties of the Eloisatron are similar to those considered for the LF or HF VLHC.

Table 1: Example parameters for heavy-ion ion colliders: gold collisions at RHIC and lead ions in LHC.

accelerator	RHIC	LHC
ion species	gold	lead
energy per charge E/Z [TeV]	0.25	7
energy per nucleon E/A [TeV]	0.1	2.76
total centre of mass E_{CM} [TeV]	39	1148
dipole field B [T]	3.46	8.4
circumference C [km]	3.83	26.66
no. of bunches n_b	57	608
number of ions per bunch N_b [10^7]	100	6.8
rms beam size at IP $\sigma^*_{x,y}$ [μm]	110	15
IP beta function $\beta^*_{x,y}$ [m]	2	0.5
tune shift per IP $\xi_{x,y}$	0.0023	0.00015
rms bunch length σ_z [cm]	18	7.5
bunch spacing $L_{\rm sep}$ [m]	63.9	124.8
rms transv. emittance $\gamma\epsilon_{x,y}$ [μm]	1.7	1.5
rms longit. emittance ϵ_L/Z [eVs]	0.12	0.2
IBS emittance growth $\tau_{\rm IBS}$ [hr]	0.4	9.8
initial luminosity L [10^{27} cm^{-2}s^{-1}]	0.2	1.0
luminosity lifetime τ [hr]	$\sim$10	9.3

2 EMPIRICAL SCALING

Figure 1 illustrates that the circumference and the dipole field are both increasing roughly with the square root of the beam energy, which implies that half of the energy gain has been realized by advances in magnet technology and the other half by expanding the real estate.

At the same time, the luminosity has roughly followed the ideal scaling, $L \propto E^2$, as is demonstrated in the left picture of Figure 2. The right picture shows that the betatron tune Q_β grows with the square root of the circumfer-

Table 2: Example parameters for pp or p$\bar{\text{p}}$ colliders: Sp$\bar{\text{p}}$S, Tevatron run IIa ('TeV2a'), LHC, LHC-II, HF VLHC, and LF VLHC. † The bunches are split in 3 trains, separated by 2.62 μs; ‡ Total LHC dipole heat load is about 0.8 W/m including the electron cloud. *Assuming a dipole packing factor 0.8 for HF-VLHC, and 0.65 for LHC and LHC-II, and ignoring possible contributions from electron cloud. ⋆Equilibrium determined by radiation damping and intrabeam scattering. Arrows refer to dynamic changes during the store. The suffix 'in' indicates initial values.

accelerator	Sp$\bar{\text{p}}$S	TeV2a	LHC	LHC-II	HF VLHC	LF VLHC
beam energy E [TeV]	0.32	0.98	7	14	50	50
dipole field B [T]	1.4	4.34	8.39	16.8	12.5	2
total energy/beam [MJ]	0.05	1	334	1320	2800	3700
circumference C [km]	6.9	6.28	26.7	26.7	89	520
number of bunches n_b	6	36	2800	5600	20000	21000
bunch population N_b [10^{11}]	1.7 (p) 0.8 ($\bar{\text{p}}$)	2.7 (p) ∼1.0 ($\bar{\text{p}}$)	1.05	1.05	0.125	0.22
no. of IPs	3	2	2 (4)	2 (4)	2	2
rms IP beam size $\sigma^*_{x,y}$ [μm]	80, 40	32	15.9	7.4⋆	9.0, 0.9	2.0
rms IP div. $\sigma^*_{x',y'}$ [μrad]	136, 272	91	31.7	34⋆	1.8	8.7
IP beta $\beta^*_{x,y}$ [m]	0.6, 0.15	0.35	0.5	0.22	5.0, 0.5	0.25
beam-beam tune shift / IP $\xi_{x,y}$	0.005	0.01	0.0034	0.005	0.0030	0.0026
crossing angle θ_c [μrad]	0	0	300	300	18	50
rms bunch length σ_z [cm]	30	37	7.7	4.0⋆	2.3⋆	20
bunch spacing $L_{\rm sep}$ [m]	1150	119 †	7.48	3.74	4.45	24.6
SR power $P_{\rm SR}$ [kW]		$< 10^{-3}$	3.6	114	492	38
dipole heat load dP/ds [W/m]		$\ll 10^{-3}$	0.2 ‡	6.6*	7.9*	0.09
betatron tune Q_β	26	∼20	63	63	115	400
rms transv. emittance $\gamma\epsilon_{x,y}$ [μm]	3.75	~ 3	3.75	3.75→1.0	1→0.3,0.03	1.0
eq. horiz. emittance $\gamma\epsilon_x^{eq}$ [μm]		~ 10⋆	2.03⋆	1.07⋆	0.29⋆	0.27⋆
longit. emittance ϵ_L (σ) [eVs]	0.11	0.11	0.2	0.15⋆	0.09⋆	1.00 (?)
damp. time $\tau_{x,\rm SR}$ [hr]		1200	52	6.5	3.3	128
IBS growth time $\tau_{x,\rm IBS}$ [hr]	10	50(?)	142	345 (in.)	224 (in.)	216
damping decrement per IP [10^{-10}]		0.025	2.5	20	190	32
events per crossing		∼6	18	90	9	50
peak luminosity L [10^{34} cm^{-2}s^{-1}]	0.0006	~ 0.02	1.00	10.	1.0	1.0
lum. lifetime τ [hr]	9	9	10	3.2	13	25

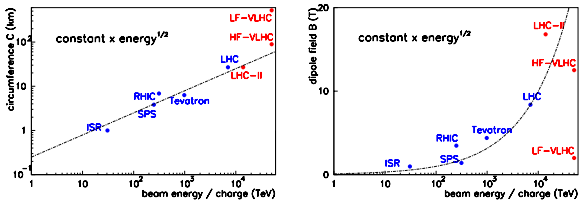

Figure 1: Left: circumference vs. beam energy; right: dipole field vs. beam energy.

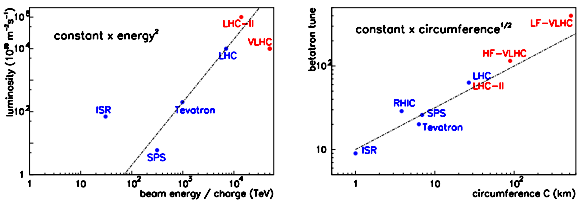

Figure 2: Left: luminosity vs. beam energy; right: betatron tune vs. circumference.

ence, implying a similar scaling for the cell length and the arc beta function [11].

3 LUMINOSITY FORMULAE

Ignoring crossing angle and hour-glass effect, the luminosity L_0 is given by

$$L = \frac{N_b^2 n_b f_{\rm rev} \gamma}{4\pi \epsilon_{x,N} \beta^*_x \kappa} \qquad (1)$$

where N_b denotes the bunch population, n_b the number of bunches per ring, $f_{\rm rev}$ the revolution frequency, γ the beam energy divided by the rest mass, $\epsilon_{x,N} = \gamma\epsilon_x$ the normalized emittance, and $\kappa = \sigma_y/\sigma_x$ the aspect ratio at the collision point. The correction factor due to crossing angle θ_c and finite bunch length σ_z can be found, *e.g.*, in Ref. [9].

An unavoidable luminosity constraint arises from the beam-beam interaction. The tune shift induced in the colli-

sion with the opposing beam is characterized by

$$\xi_{x,y} = \frac{\beta^*_{x,y} r_A N_b}{2\pi\gamma\sigma^*_{x,y}(\sigma^*_x + \sigma^*_y)} \qquad (2)$$

where $r_A = Z^2e^2/(4\pi\epsilon_0 A m_p c^2)$ is the classical particle radius, A the mass of the ion in units of the proton mass, and Z the charge in units of e. Below we assume that $\beta^*_y/\beta^*_x = \epsilon_y/\epsilon_x = \kappa$, since this gives the maximum tune shift in both planes: $\xi_x = \xi_y \equiv \xi$. Using the beam-beam parameter ξ, we can rewrite the luminosity, Eq. (1), as

$$L = (f_{\rm rev} n_b N_b)\,\frac{1+\kappa}{\beta^*_y}\,\gamma\frac{\xi}{2r_A}. \qquad (3)$$

The first factor, in parentheses, is the total beam current. Three further variables are the IP beta function $\beta^*_y = \beta^*_x\kappa$, the emittance ratio κ, and the maximum beam-beam tune shift ξ. For flat beams ($\kappa \ll 1$) the luminosity is a factor of two lower than for round beams ($\kappa = 1$), unless smaller values of $\beta^*_y = \kappa\beta^*_x$ can be achieved. This seems difficult in proton-proton collisions, where both beams pass through the same low-β triplets [10].

In Section 4, we consider limits on the IP beta functions. Section 5 addresses the effects of synchrotron radiation and intrabeam scattering, and, in particular, the variation of beam parameters during the store. Interplay of radiation damping and collective instabilities is examined in Section 6. In Section 7, we investigate bounds on the total beam current, before we draw conclusions in Section 8.

4 MINIMUM β^*

The IP beta function should be larger than the rms bunch length, $\beta^*_{x,y} \geq \sigma_z$, to avoid luminosity reduction due to the hourglas effect. A tighter limit on $\beta^*_{x,y}$ arises from long-range beam-beam encounters at parasitic collision points on both sides of the IP.

In order to ensure a sufficient dynamic aperture caused by parasitic collisions, the separation of the two beams should be $n_{\rm sep} \geq 10$. For the LHC, this separation results in a dynamic aperture of about 8σ [12]. On the other hand, to avoid luminosity degradation due to the crossing, not included in Eq. (1), the total crossing angle θ_c should be smaller than $2\sigma_x/\sigma_z$. Combining these two requirements, we find $\beta^*_x \geq n_{\rm sep}\sigma_z/2 \approx 5\sigma_z$. For the LHC, this limit evaluates to about 0.38 m, not far from the design beta function of 0.5 m.

The long-range collisions induce additional tune shifts; see Fig. 3 (left picture). The LHC beams are crossed alternatingly in the horizontal and vertical plane at the various IPs, so that the long-range tune shifts induced at different IPs approximately cancel each other [13]. In this case the tighter limit on the beta function applies for both planes,

For flat beams the beta functions are unequal, and the long-range beam-beam tune shift in the vertical plane is enhanced by a factor $1/\kappa$ [11],

$$\Delta Q^{LR}_y = -\frac{1}{\kappa}\Delta Q^{LR}_x = \frac{1}{\kappa}\frac{n_{LR}}{n^2_{\rm sep}}\,\xi, \qquad (4)$$

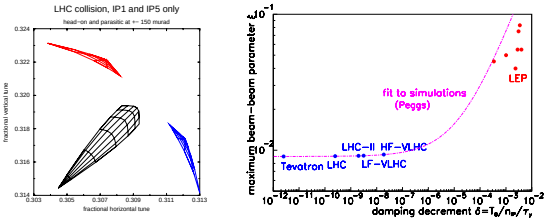

Figure 3: Left: tune footprints due to head-on and long-range beam-beam effects in LHC IPs 1 and 5, respectively (courtesy H. Grote); right: tune shift parameter vs. damping decrement δ (LEP data courtesy of R. Assmann).

where n_{LR} denotes the total number of parasitic collisions on either side of the interaction point, and $n_{\rm sep} = \theta_c/\sigma_{x'}$ the normalized separation. In view of Eq. (4), the cancellation of tune shifts between IPs is not possible at flat-beam colliders. However, advanced techniques to compensate effects of the long-range collisions, using either an electron lens with modulated current [14] or pulsed electric wires [15], would be applicable to flat beams as well.

Limits on the beta functions could also arise from optical considerations, such as the available aperture, maximum quadrupole gradients, and chromaticity [16]. For all hadron colliders in Tables 1 and 2 these optical limits are much looser than those imposed by the long-range collisions. They may be relaxed even further by decreasing energy spread (adiabatic and radiation damping), and by novel final-focus concepts [17].

5 EMITTANCE

Already at the LHC, radiation damping surpasses the intrabeam scattering growth rate. For post-LHC hadron colliders, synchrotron radiation may decide the choice of machine parameters. The energy loss per turn is $U_0 = C_\gamma E^4/\rho$ where ρ is the bending radius, E the beam energy, and $C_\gamma \approx 4\pi/3\ r_A/(m_Ac^2)^3 \approx 0.778 \times 10^{-17}\ Z^2/A^4{\rm m/GeV}^3$. The product of amplitude damping time and partition number is [18]

$$\tau_z J_z = \left(\frac{3(m_Ac^2)^3}{e^2c^3r_AZ^2}\right)\frac{1}{B^2E}\left(\frac{C}{2\pi\rho}\right) \qquad (5)$$

where z labels either plane, and $C/(2\pi\rho)$ denotes the reciprocal of the dipole filling factor. The damping time decreases inversely with energy and the square of the dipole field.

A maximum tune shift of 0.009 was achieved at the Tevatron, where radiation damping is negligible and the two beams have unequal emittances. Strong radiation damping would allow for larger beam-beam tune shifts. Both measurements and simulations have been fitted by [19] $\xi_{\rm max} \propto 0.009 + 0.021\ (\delta/10^{-4})^{0.5}$, where $\delta = T_0/(n_{\rm IP}\tau_{x,y})$ is the damping decrement, $T_0 = 1/f_{\rm rev}$ the revolution period and $\tau_{x,y}$ the transverse damping time. In order to attain a noticeable gain, the damping decrement must be at least 10^{-4}, and for $\delta \approx 10^{-3}$ the

beam-beam tune shift limit increases by an order of magnitude. Using Eq. (5), $\rho = E/(ZeBc)$, and $n_{\rm IP} = 2$, we rewrite the damping decrement as $\delta \approx 5.7 \times 10^{-13}\, E[\mathrm{TeV}]^2 B[\mathrm{T}] Z^3/A^4$. In all our examples, δ is far too small to affect the beam-beam limit; see Table 2 and the right picture in Fig. 3.

A more important consequence of the synchrotron radiation is the shrinkage of the beam, which allows for higher luminosity. The situation differs from electron storage rings in that, even at highest energies presently envisioned, the damping times are still of the order of hours and not milliseconds. Therefore, the synchrotron radiation likely leads to a continuous change of the beam emittance during the store. For a careless choice of parameters, this may result in unwantedly high beam-beam tune shifts, consequent blow-up, halo generation and background.

In electron storage rings, an equilibrium emittance is established as a balance of quantum excitation and damping. The corresponding normalized emittance is [18]

$$\epsilon_{x,N}^{\rm SR} \approx \frac{55}{32\sqrt{3}} \frac{\lambda\!\!\!^{-}_A}{J_x} \left(\frac{\gamma^3}{Q_\beta^3}\right) \left(\frac{C}{2\pi\rho}\right)^3 \qquad (6)$$

where $\lambda\!\!\!^{-}_A = \hbar/(m_A c)$ is the Compton wavelength of the particle ($\lambda\!\!\!^{-}_A \approx 2.1 \times 10^{-16}/A$ m). We have employed the smooth approximations $\beta_{x,y} \approx C/(2\pi Q_\beta)$, $\hat{D} \approx \beta^2/\rho$ and $\mathcal{H} \approx \beta^3/\rho^2 \approx \rho/Q_\beta^3$ $(C/(2\pi\rho))^3$, which we use throughout this paper. For LHC-II parameters, the horizontal equilibrium emittance is about 3 orders of magnitude smaller than the design emittance, for the HF VLHC the difference is still a factor 10–100.

Thus, for any reasonable bunch current, the equilibrium emittance will not be determined by quantum fluctuations, but instead it will result from a balance of radiation damping and intrabeam scattering. For $\gamma \gg 1$, the horizontal emittance growth rate, $1/\tau_{x,\rm IBS} \equiv 1/\sigma_x\, d\sigma_x/dt$, due to intrabeam scattering (IBS) is [20]

$$\frac{1}{\tau_{x,\rm IBS}} \approx \frac{c r_A^2 N_b A L_c}{16 Q_\beta \epsilon_{x,N}^2 \sqrt{\kappa}\sqrt{\kappa+1}\gamma\sigma_z\sigma_\delta} \qquad (7)$$

where L_c ($L_c \approx 20$) denotes a Coulomb logarithm.

Asymptotically, for $\gamma \gg Q_\beta$, the longitudinal growth rate $1/\tau_{\delta,\rm IBS} \equiv 1/\sigma_\delta\, d\sigma_\delta/dt$ approaches the same value as $1/\tau_{x,\rm IBS}$, and the rms relative momentum spread becomes $\sigma_\delta \approx Q_\beta^{3/2}\sqrt{\epsilon_x/\rho}$. Combining this with Eqs. (5), (7), and $\sigma_s = c\alpha_c/\Omega_s\sigma_\delta$ (Ω_s is the synchrotron frequency), we can solve for the equilibrium emittance:

$$\epsilon_{x,N}^{\rm IBS} = \frac{\rho^{5/6} N_b^{1/3}}{Q_\beta \gamma^{7/6}} \left(\frac{Z f_{\rm rf} e V_{\rm rf}}{c E_A \kappa(\kappa+1)}\right)^{1/6} \qquad (8)$$

$$\left(\frac{C}{2\pi\rho}\right)^{1/6} \left(\frac{3 r_A L_c A}{16}\right)^{1/3}, \qquad (9)$$

where $f_{\rm rf}$ is the rf frequency and $V_{\rm rf}$ the total rf voltage.

In a flat-beam configuration, the horizontal and longitudinal emittances may already halt their decline, while the vertical emittance ϵ_y continues to decrease, until it approaches a value $\kappa\epsilon_x$, where κ is determined by linear coupling and spurious vertical dispersion. Following Keil [18], we assume that LHC-II is operated on or near the coupling resonances, so that the horizontal and vertical emittances are approximately equal.

Assuming a total rf voltage of 45 MV at 400 MHz, $\kappa = 1$ for LHC-II and LF-VLHC, $\kappa = 0.1$ for the HF-VLHC, and $J_{x,y} = 1$, we obtain the equilibrium emittances and bunch lengths listed in Table 2. Since the equilibrium emittance depends on the beam current, which, in collision, decays on a time scale comparable to the damping time, no real steady state is established, and the luminosity lifetime is longer than it would be for constant emittances. Figure 4 illustrates the simulated variation of emittances, beam current, beam-beam tune shifts and luminosity during a 10-hr store in LHC-II. The simulation includes radiation damping, intrabeam scattering, and particle consumption in collisions at two IPs. The maximum tune shift approaches 0.005. This is only half the peak value reached at the Tevatron. Emittance evolution and tune shift excursions could be further optimized. A constant beam-beam tune shift may be maintained, *e.g.*, by varying the damping partition numbers and the IP beta functions during the store.

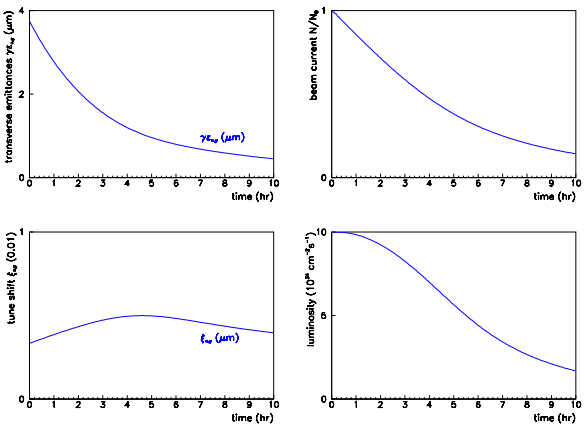

Figure 4: Dynamic changes during a store in LHC-II for the parameters of Table 2 and damping partition numbers $J_x = J_y = 1$, $J_s = 2$; emittances (top left), beam current (top right), beam-beam tune shifts (bottom left), and luminosity (bottom right) vs. time.

6 COLLECTIVE EFFECTS

If the coherent synchrotron tune shift exceeds the tune spread due to the rf curvature, Landau damping is lost for higher-order longitudinal modes. Introducing the effective impedance $(Z_L/n)_{\rm eff}$ and harmonic number $h_{\rm rf}$ the condition for stability is [21, 22]

$$\sigma_s \geq \frac{C}{2\pi}\left[\frac{\pi^3}{6}\frac{N_b f_{\rm rev} e}{h_{\rm rf}^3 V_{\rm rf}}\,\mathrm{Im}\left(\frac{Z_L}{n}\right)_{\rm eff}\right]^{1/5}. \qquad (10)$$

If synchrotron radiation damping reduces the rms bunch length, the beam could become unstable during the store. An example for the LHC-II parameters is shown in the left picture of Fig. 5. Assuming an effective impedance of $\mathrm{Im}(Z_L/n)_{\mathrm{eff}} \approx 0.1\ \Omega$, similar to the present LHC value, Landau damping is lost after about 3 hours. One approach of maintaining a bunch length above the threshold is longitudinal excitation using 'pink noise' [23]. The bunch-length evolution for such scenario is shown on the right.

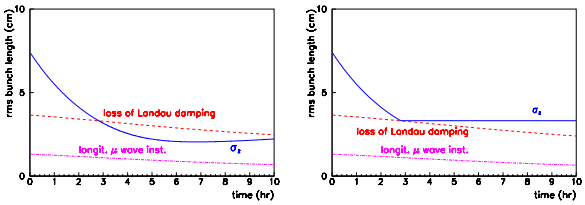

Figure 5: Evolution of the rms bunch length during a store in LHC-II compared with the threshold values for loss of Landau damping, Eq. (10) and for longitudinal microwave instability [22], for the same parameters as in Fig. 4 (left) and when after 3 hours noise is added to maintain a constant value $\epsilon_L \geq 0.104$ eVs (right).

For rings with large circumference coupled-bunch instabilities driven by the resistive wall are also a concern [18, 21]. Another problem is the electron cloud [5].

7 TOTAL BEAM CURRENT

The first term on the right hand side of Eq. (3) is associated with the total beam current. This may be limited by the sustainable synchrotron radiation power,

$$P_{\mathrm{SR}} = \frac{C_\gamma E^4 N_b n_b c}{C\rho} = U_0 f_{\mathrm{rev}} n_b N_b, \qquad (11)$$

which, using Eq. (5), can be rewritten as [18]

$$P_{\mathrm{SR}} = \left(\frac{8\pi r_A^{3/2}}{\sqrt{3cE_A}}\right) \frac{\kappa}{1+\kappa^2} \frac{E^{3/2} L \beta_x^*}{\xi \sqrt{J_z \tau_z}} \sqrt{\frac{C}{2\pi\rho}}. \qquad (12)$$

For a constant dipole field B, we obtain $J_z\tau_z \propto 1/E$ and $P_{\mathrm{SR}} \propto E^2 L$, whereas for $B \propto E^{1/2}$, the damping time shortens as $J_z\tau_z \propto 1/E^2$, and the s.r. power increases as $P_{\mathrm{SR}} \propto E^{5/2} L$. These scaling laws are more pessimistic than those derived in VLHC studies [11]. If the wall-plug power required for cryogenics is about 30 times the radiation power P_{SR} [11], it stays below 20 MW for all projects considered here. In Table 2 the maximum values for the power per unit length are a factor of 4–6 above the LHC cooling capacity, which can be taken care of, *e.g.*, by increasing the beam-screen temperature.

8 CONCLUSIONS

Hadron colliders have performed exceedingly well in the past. Profiting from enhanced synchrotron radiation, they hold the promise of further substantial advancements in energy and luminosity at sustainable power levels and costs.

9 ACKNOWLEDGEMENTS

I thank J. Gareyte, R. Assmann, P. Bagley, M. Battaglia, O. Brüning, H. Burkhardt, W. Fischer, O. Gröbner, H. Grote, G. Guignard, W. Herr, J.B. Jeanneret, J. Jowett, E. Keil, J.-P. Koutchouk, S. Peggs, F. Pilat, F. Ruggiero, G. Rumolo, F. Schmidt, R. Schmidt, E. Shaposhnikova, R. Thomas, A. Verdier, R. v. Weelderen, and J. Wei for discussions and informations.

10 REFERENCES

[1] E. Keil, "Intersecting Storage Rings," CERN 72-14, 1972.

[2] A. Hofmann, et al., CERN ISR-OP-TH/80-19, 1980.

[3] L. Evans, 1987 IEEE PAC, Washington, 1987; M. Harrison, R. Schmidt, EPAC 88 Nice, 1988; V. Hatton, 1991 IEEE PAC, San Francisco, 1991.

[4] G. Dugan, 14th HEACC, Tsukuba, 1989.

[5] K. Ohmi, Phys. Rev. Lett. 75, 1526, 1995; F. Zimmermann, CERN LHC PR 95, 1997; O. Gröbner, IEEE PAC97 Vancouver; K. Ohmi, F. Zimmermann, Phys. Rev. Lett. 85, 3821, 2000; G. Rumolo et al., PRST-AB 012801, 2001; CERN SL workshops Chamonix X & XI, 2000 and 2001.

[6] S. Klein, LBL-PUB-45566, 2000; J.B. Jeanneret, SL/AP Beam Physics Note 41; D. Brandt, LHC Project Report 450, 2000.

[7] See web site *http://vlhc.org*

[8] A.G. Ruggiero, Hadron Colliders at Highest Energies and Luminosities, World Scientific, Singapore, 1998.

[9] K. Yokoya, P. Chen, 1990 US-CERN School, Springer.

[10] E. Keil, private communication (2001).

[11] A. Chao, S. Peggs, R. Talman, presentations at Mini-Workshop: "The effect of synchrotron radiation in the VLHC," BNL, Sept. 18–20, 2000.

[12] J. Irwin, SSC-233, 1989; Y. Papaphilippou et al., PRST-AB 2, 104001, 1999.

[13] D. Neuffer, S. Peggs, SSC-63, 1986; W. Herr, CERN-SL/90-06 AP, 1990.

[14] V.D. Shiltsev et al., PRST-AB, 2:071001,1999

[15] J.-P. Koutchouk, LHC PN 223; submitted to PAC2001.

[16] E.D Courant and E. Keil, Proc. Batavia 1978; E. Keil, Joint US-CERN School, Benalmadena 1992.

[17] P. Raimondi and A. Seryi, LINAC2000, Monterey, 2000.

[18] E. Keil, "Synchotron Radiation Dominated Hadron Colliders," Proc. PAC 97, p. 104, 1996, and Proc. 34th Eloisatron Workshop, Erice 1996.

[19] E. Keil and R. Talman, Particle Accelerators vol. 14, 1993; S. Peggs, LHC99 beam-beam workshop, Geneva, 1999; R. Assmann and K. Cornelis, EPAC 2000 Vienna, 2000.

[20] J. Wei, "Intrabeam Scattering Scaling for Very Large Hadron Colliders," unpublished draft (2001); J. Bjorken and S. Mtingwa, Part. Acc. 13, 115 (1983).

[21] F. Ruggiero, CERN SL/95-09, 1995.

[22] J.T. Rogers, CBN 96-14, 1996.

[23] T. Toyama, et al., Proc. EPAC 2000, Vienna; similar methods were used at the S$p\bar{p}$S by T. Linnecar.